arXiv:1302.4768v2 [cond-mat.mes-hall] 22 Feb 2013

Berry phase interference and single-electron transport in a three-ion magnetic molecule

Javier I. Romero* and Eduardo R. Mucciolo†
Department of Physics, University of Central Florida, Orlando, Florida 32816, USA

(Dated: February 26, 2013)

We study single-electron transport in a magnetic molecule by using a stationary rate equation approach. In the molecule, two magnetic ions and are connected to each other through a third, nonmagnetic ion. The magnetic ions are coupled to ideal metallic leads and a back gate voltage is applied to the molecule, forming a field-effect transistor. A Hamiltonian which includes inter-ion hopping, on-site repulsion, and magnetic anisotropies is employed to describe this molecule, resulting in an energy spectrum similar to that of single molecule magnets in the giant-spin approximation. An external in-plane magnetic field is then used to drive the molecule to a diabolical point, where states with maximum total spin with opposite directions are degenerated. Both linear and nonlinear transport are evaluated near the diabolical point, showing features that can be attributed to Berry-phase interference of spin tunneling paths.

I. INTRODUCTION

From the various types of magnetic states in matter, ferromagnetism and its microscopic causes is one of the most intriguing topics. A very singular class of magnetic systems are single-molecule magnets (SMMs).[1–3] Molecules in this class typically have a large net spin ground state and exhibit unusual attributes such as quantum tunneling of the magnetization (QTM),[4,5] a relatively large decoherence time,[6] and Berry-phase interference effects in the presence of magnetic fields.[7,8] Commonly, SMMs are composed of transition metal ions (open $3d$ or $4f$ shells) bridged by ligand atoms and molecules. The Hamiltonian that describes well the magnetic properties of SMMs is the so-called giant spin approximation (GSA) model. For instance, in its simplest form, the GSA Hamiltonian can be written as

$$H_{\mathrm{GSA}} = -D\, S_z^2 + E\, \left(S_x^2 - S_y^2\right), \tag{1}$$

The net magnetization has a preferential direction (an easy axis z in this example) as a consequence of the dominant uniaxial anisotropy ($D \ll E$). The in-plane transverse anisotropy allows the total spin to transit between different values of S_z. In this particular example, the molecule has a predominant second-order anisotropy signaling a rhombic symmetry.

A more microscopic description of SMMs comes from considering interactions at the ion level. In this case, one uses instead a multi-spin Hamiltonian of the type

$$H_{\text{multi-spin}} = \sum_i \left[-d_i S_z^2 + e_i \left(S_x^2 - S_y^2\right)\right] - \sum_{i\neq j} J_{ij} \vec{S}_i \cdot \vec{S}_j, \tag{2}$$

Here, each magnetic site of the molecule has itself local uniaxial and transverse anisotropies d_i and e_i, respectively. In addition, there is an effective ferromagnetic interaction between pairs of sites parameterized by J_{ij}. Both models have been compared in Ref. 9. For zero transverse anisotropies ($e_i = E = 0$), the diagonalization of the Hamiltonians in Eqs. (1) and (2) yield a two-fold degenerate ground state involving spin states parallel ($S_z = S$) and anti-parallel ($S_z = -S$) to the uniaxial anisotropy axis. If the transverse anisotropy terms (e_i and E) are nonzero, then rotational S_z symmetry is broken and the two-fold degeneracy is lifted, with the ground and first excited states being antisymmetric and symmetric combinations of the $S_z = \pm S$ states. In theoretical studies, due to the large Hilbert space involved and the strong interplay between the many microscopic parameters, it is very challenging to take into account explicitly the overlap between orbitals and their symmetries in magnetic molecules. One often employs the empirical Goodenough-Kanamori rules[10,11] that dictate the nature of interaction between magnetic ions. In addition, one also includes an effective interaction intermediated by diamagnetic atoms (the Anderson superexchange interaction).[12]

In recent years, interest emerged in exploring how the magnetic properties of SMMs may affect the molecule's electronic transport properties. Effects due to the QTM[13] and Berry-phase interference[14,15] and their interplay with the Kondo resonance[16,17] have been proposed. Several authors have also used first-principles calculations to investigate the electronic configuration, the magnetic properties, and coherent transport in SMMs.[18–21]

In this paper, we investigate the dependence of sequential tunneling transport on an applied transverse magnetic field in a three-ion model that contains the essential microscopic details necessary for reproducing a SMM behavior. The microscopic model comprises two magnetic ions bridged by a third diamagnetic ion. The microscopic model takes into account the valence, ligand fields, and orbital energies of the ions, as well as direct and exchange Coulomb interactions present in the molecule. Our goal is to develop a simple yet phenomenologically complete microscopic model of a SMM that goes beyond the giant spin Hamiltonian model and is amenable to realistic electronic transport studies.

We explore the energy spectrum of this system for several points in the parameter space of the Hamiltonian. We find that for a certain parameter range a magnetic bistability, similar to that of SMMs, develops. We then focus our attention on Berry-phase interference effects on the single-electron transport through the molecule since this is one of the most unusual features expected of a SMM. In our calculations, transport is evaluated under an applied transverse magnetic field whose magnitude and direction are tuned with respect to a diabolical point (see Ref. 22). At the diabolical point, Berry-phase destructive interference of spin paths of the molecule is maximal, completely compensating the mixing of opposite spin orientations brought by the in-plane anisotropy. As a result, the ground-state degeneracy of spin states is restored..

The paper is organized as follows: In Sec. II we describe the model Hamiltonian for the three-ion magnetic molecule. In Sec. III presents our choice of model parameters and the energy spectrum and symmetry of the states of the molecule in the absence and in the presence of transverse anisotropy and magnetic field terms. In Sec. IV we evaluate the incoherent sequential current and differential conductance of the molecule for zero field and for a nonzero field tuned near the diabolical point. In Sec. V, we discuss the effects of Berry phase interference on transport, which are most visible in the molecule's differential conductance. Finally, in Sec. VI, we analyze our results and draw some conclusions.

II. THE THREE-ION MODEL OF A SMM

A minimal realistic molecular core capable of reproducing the main features of a SMM such as large total spin ($S > 1/2$), uniaxial and in-plane anisotropies, and Berry-phase interference consists of two transition metal ions bridged by a diamagnetic ligand ion. Consider the system shown schematically in Fig. 1. The two transition metal ions a and c have a $3d^8$ electronic configuration and a total spin $S = 1$ each. They interact magnetically through a superexchange interaction intermediated by a diamagnetic O^{2-} ion (electronic configuration $2p^6$), represented by b in Fig. 1. The five-fold degeneracy of the $3d$ orbitals in the magnetic ions is broken due to the bonding to ligands. To simulate such an effect, we assume that a weak orthorhombic field acts on a and c, inducing identical local uniaxial and transverse anisotropies on each site. Thus, for an orthorhombic symmetry (D_{2h} point group), the ground states of ions a and c have two occupied unpaired single-particle orbitals ($a_{1,2}$ and $c_{1,2}$, respectively) which are symmetric and antisymmetric combinations of $d_{x^2-y^2}$ and $d_{3z^2-r^2}$ d states. We also consider a 90° angle between their bonds. As a result, the $d_{x^2-y^2}$ components of the single-particle orbitals in both ions a and c overlap separately with the $p_{x,y}$ orbitals $b_{1,2}$ of ion b. Under this assumption, we use the appropriate Slater-Koster two-center integrals, which then yields $E_{p_x,d_{x^2-y^2}} = E_{p_y,d_{x^2-y^2}} = (pd\sigma)\sqrt{3}/2$. This configuration favors a ferromagnetic superexchange interaction. In our case the σ two-center integrals are zero.

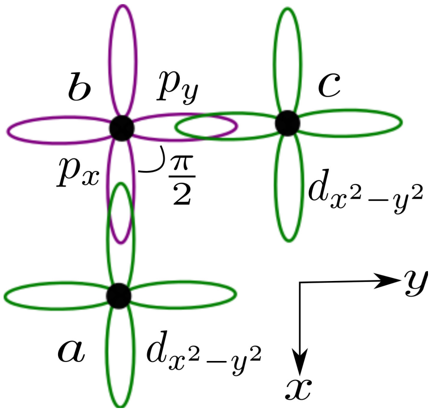

Figure 1: (Color online) Scheme of a simple three-ion SMM. The magnetic ions labeled by a and c interact through the diamagnetic ligand ion b with a bond angle of $\theta = \pi/2$, so that the $d_{x^2-y^2}$ orbitals (green/solid lobes) overlap with the p_x and p_y orbitals (purple/dasher lobes) of the ligand separately.

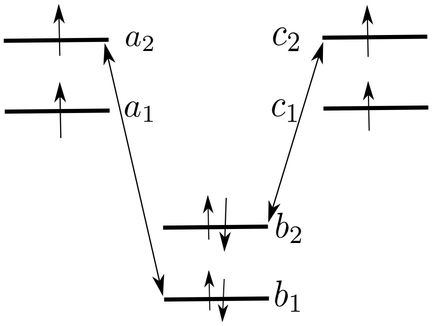

Figure 2: Scheme of the electron hopping (double-arrow lines) between magnetic ions and the ligand's orbitals. For a $3d^8$ ion in a weak orthorhombic ligand field, the unpaired single-particle orbitals (say for ion a) are $\psi_{a_2} = \kappa_1\, d_{x^2-y^2} + \kappa_2\, d_{3z^2-r^2}$ and $\psi_{a_1} = \kappa_1\, d_{3z^2-r^2} - \kappa_2\, d_{x^2-y^2}$, where $\kappa_1^2 + \kappa_2^2 = 1$. We regard κ_2 as a small parameter: $|\kappa_2| \ll |\kappa_1|$.

The scheme of these selective orbital overlaps is shown in Fig. 2. The features of our model are captured by the effective Hamiltonian

$$H_{\text{molecule}} = H_a + H_b + H_c + H_{ab} + H_{bc} \tag{3}$$

where

$$\begin{aligned} H_\alpha &= \sum_{i=1,2} \varepsilon_{\alpha_i}\, n_{\alpha_i,\sigma} + U_\alpha \sum_{i=1,2} n_{\alpha_i,\uparrow}\, n_{\alpha_i,\downarrow} \\ &\quad + U'_\alpha \sum_{\sigma,\sigma'=\uparrow,\downarrow} n_{\alpha_1,\sigma}\, n_{\alpha_2,\sigma'} - J_\alpha\, \vec{S}_{\alpha_1} \cdot \vec{S}_{\alpha_2} \\ &\quad - d_\alpha\, S_{z,\alpha}^2 + e_\alpha \left(S_{x,\alpha}^2 - S_{y,\alpha}^2 \right), \end{aligned} \tag{4}$$

with $\alpha = a, b, c$ and $d_b = e_b = 0$,

$$\begin{aligned} H_{ab} &= t \sum_{\sigma=\uparrow,\downarrow} \left(c_{a_2,\sigma}^\dagger\, c_{b_1,\sigma} + \text{H.c.} \right) \\ &\quad + t' \sum_{\sigma\neq\sigma'} \left(c_{a_2,\sigma}^\dagger\, c_{b_1,\sigma'} + \text{H.c.} \right), \end{aligned} \tag{5}$$

and

$$H_{bc} = t \sum_{\sigma=\uparrow,\downarrow}\left(c^{\dagger}_{b_2,\sigma}\, c_{c_1,\sigma} + \text{H.c.}\right) + t' \sum_{\sigma\neq\sigma'}\left(c^{\dagger}_{b_2,\sigma}\, c_{c_1,\sigma'} + \text{H.c.}\right). \qquad (6)$$

In Eqs. (4), (5), and (6), $n_{\alpha_i,\sigma} = c^{\dagger}_{\alpha_i,\sigma} c_{\alpha_i\sigma}$, where $c^{\dagger}_{\alpha_i,\sigma}$ ($c_{\alpha_i\sigma}$) creates (annihilates) an electron with z spin projection σ in the orbital i of ion α and follow the standard fermionic anticommutation relations. The total spin operator associated to the orbital i in ion α is $\vec{S}_{\alpha_i}$ while $\vec{S}_{\alpha} = \vec{S}_{\alpha_1} + \vec{S}_{\alpha_2}$.

In Eqs. (5) and (6), we include both spin preserving and spin flipping hopping terms. In Eq. (4), the first term accounts for the filling of the single-particle orbitals, while the second and third terms represent the on-site Coulomb repulsion. The fourth term enforces Hund's first rule, maximizing the total spin on each ion ($J_\alpha > 0$), and the last two terms are the uniaxial and transverse on-site anisotropies produced by the rhombic ligand field environment and by the spin-orbit coupling within each magnetic ion. Typically, $|d_\alpha| > |e_\alpha|$.

III. ADJUSTING THE MODEL PARAMETERS

The model Hamiltonian in Eq. (3) has a large number of parameters that have to be properly adjusted in order to produce the phenomenology expected of a SMM. Below, we discuss our choices of parameter values. We first consider the Hamiltonian in the absence of transverse anisotropy ($e_\alpha = 0$ and $t' = 0$). Then we include transverse anisotropy and the coupling to an in-plane external magnetic field in order to produce diabolical points in the spectrum of the molecule.

A. Total S_z spin in the absence of transverse anisotropy and of spin-flip hopping

The eigenvalues and eigenstates of the Hamiltonian in Eq. (3) are very sensitive to the values of its parameters. A convenient way to produce a spectrum similar to those of SMMs is to start with S_z as a good quantum number by setting $e_\alpha = t' = 0$. Then, one considers how the eigenstate amplitudes resemble the Clebsch-Gordan amplitudes obtained for two $S = 1$ particles when different choices of parameters t, ε_{α_i}, U_α, U'_α, J_α, and d_α are used. Due to the molecule's symmetry, we can assume $\varepsilon_{a_i} = \varepsilon_{c_i} = \varepsilon_i$, $U_a = U_c = U$, $U'_a = U'_c = U'$, $J_a = J_c = J$, and $d_a = d_c = d$. For simplicity we have set $U_b = U'_b = 0$. The single-particle orbital energies of the bridging ion are set as $\varepsilon_{b_1} = \varepsilon_{b_2} = \varepsilon_b$.

Realistic values for some parameters can be obtained from the review by Imada, Fujimori, and Tokura[23] and the recent work by Kim and Min.[24] We set the on-site and intraorbital Coulomb interactions to $U = 7$ eV and $U' = 4.5$ eV, respectively. The Hund's rule parameters are $J = 0.95$ eV and $J_b = 1.3$ eV. The orbital energies have the values $\epsilon_1 = 0.71$ eV, $\epsilon_2 = 0.72$ eV, and $\epsilon_b = 0.05$ eV.

The uniaxial anisotropy parameter is set to $d = 58\,\mu$eV (0.67 K). For this particular choice of parameter values, we calculate the total S_z spin of the molecule. Figure 3 shows $|S_z|$ for the ground state (two-fold degenerate), first excited state (two-fold degenerate), and second excited state (nondegenerate) versus the hopping parameter t. It is clear that for the range of values probed, the ground state has the highest possible total spin, $S = 2$. For $t > 1.2$ eV, the states with total spin $S = 1$ become the first excited states, while the state with total spin zero moves up to the second excited state position. This is the typical case for a SMM within the description provided by the giant spin Hamiltonian of Eq. (1).

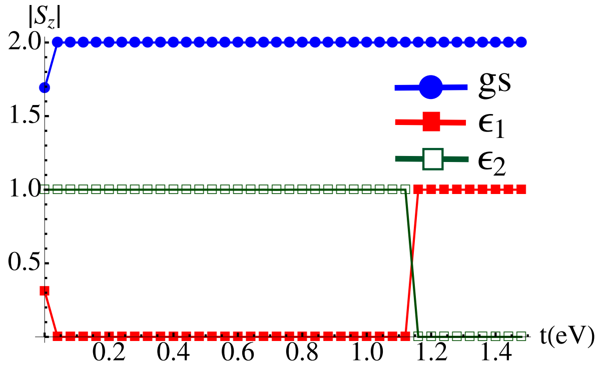

Figure 3: (Color online) Total S_z spin of the molecule. For $0 < t < 1.19$ eV, the lowest energy level is a $|\pm 2\rangle$ state, the first excited state has $S_z = 0$, while the next (degenerate) excited states have $S_z = \pm 1$. We find the typical SMM behavior in the $1.2\,\text{eV} < t < 1.5$ eV range, where the first excited states have $S_z = \pm 1$ and the highest energy level has $S_z = 0$. The crossing in the graph denotes the point where total S_z spin changes for the first and second excited eigenstates. For $t = 1.5$ eV, the energy splitting between the two lowest eigenstates ($S_z = \pm 2$ and $S_z = \pm 1$) is of the order of the uniaxial anisotropy parameters d_α, with the value of $\Delta = 57\,\mu$eV, while the splitting between $S_z = \pm 1$ and $S_z = 0$ is $\Delta = 8.43\,\mu$eV.

B. Anisotropy and diabolical points

We now consider the inclusion of anisotropy terms, which make the eigenstates to be symmetric and antisymmetric combinations of $|S_z\rangle$ states. In addition, we consider the effect of an applied transverse (in-plane) magnetic field on the molecule's energy spectrum. The transverse field Hamiltonian is given by

$$H_{\text{field}} = b\left(\sum_{\alpha=a,c} g_{x,\alpha} S_{x,\alpha}\cos\phi + g_{y,\alpha}\, S_{y,\alpha}\sin\phi\right), \qquad (7)$$

where $b = \mu_B|\vec{B}|$ and $\vec{B} = (B\cos\phi, B\sin\phi, 0)$ is the external magnetic field. Following Refs. 25 and 26, a reasonable estimate of the anisotropic g-factors would be $g_{x,\alpha} = 2.270$ and $g_{y,\alpha} = 2.269$. We set the spin conserving hopping parameter to $t = 1.5$ eV, while the spin-flipping and transverse anisotropy parameters are set to $t' = 9\,\mu$eV and $e_a = e_c = 0.17d$, respectively. We do not consider coupling of the magnetic field to the middle ion since it would change the energy levels of the high energy sector by a very small amount, given that $b \ll U$. In Fig. 4, we show the resulting splitting of the two lowest energy levels versus the angle ϕ, while in Fig. 5 the splitting is shown as a function of the applied field magnitude b. The angle $\phi = \pi$ creates symmetric spin paths for the tunneling of the molecule's magnetization, leading to maximum destructive interference. It is at this particular direction that we plot the energy splitting in Fig. 5. The periodic modulation of the splitting with b is a characteristic feature of SMMs (see Refs. 4,7,27). The separation between successive zeros of the splitting for a system described by the GSA [Eq. (1)] under a field $h_{\text{field}} = -g_x b$ (with $b = \mu_B B$) is given by $\Delta b_{\text{gsa}} = (2/g_x)\sqrt{2E(E+D)}$. Note that using this expression and our choice of values for the anisotropy parameters e and d, the predicted period of the oscillation would be $\Delta b_{\text{gsa}} = 32.2\,\mu$eV, which is not in agreement with the actual value of $\Delta b \approx 8.5\,\mu$eV obtained from Fig. 5. The derivation of an analytical expression for the period of the splitting may not be possible for our Hamiltonian and we do not attempt it here. In the following, we will the fix the direction of the field to $\phi = \pi$ and only consider the dependence with respect to the field magnitude b.

We now consider how the symmetry and energy of the eigenstates are affected by changes in the magnitude of the magnetic field. For this purpose, we define the symmetry coefficient

$$C_\Sigma = \frac{1}{2}|C_1 + C_2|, \tag{8}$$

where $C_{1,2}$ are the amplitudes of the two degenerate states along the $S_z = \pm 2$ basis states. If $C_\Sigma = 0$ the eigenstate is antisymmetric, whereas if $C_\Sigma = C_{1,2}$ the eigenstate is symmetric. The results are presented in Fig. 6. We observe that the ground state changes from symmetric to antisymmetric at the first diabolical point (left dashed line), while the first excited state does the reverse. The energy splitting between the linear combination of S_z states (symmetric and antisymmetric) vanishes at the diabolical points, since the two lowest energy states become degenerate at those points.

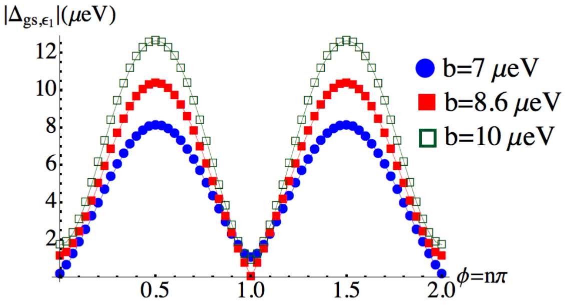

Figure 4: (Color online) Splitting of the two lowest energy levels versus the transverse field angle ϕ. The angle is measured with respect to the positive x axis. We see that for various values of the magnetic field, the lowest splitting occurs at $\phi = \pi$.

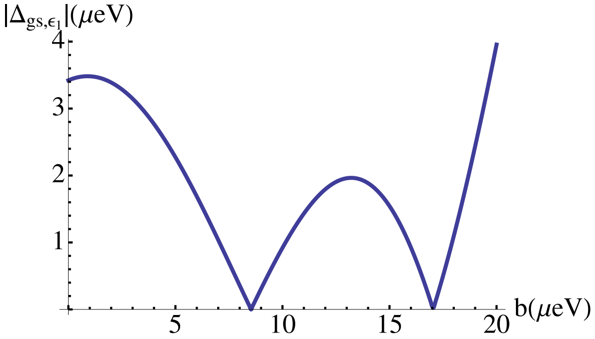

Figure 5: (Color online) Splitting of the two lowest energy levels versus the magnitude of the magnetic field b at an angle of $\phi = \pi$. We observe two diabolical points where the splitting between the two lowest energy levels goes to zero. The first diabolical point occurs at $b \approx 8.5\ \mu$eV ($B \approx 0.14$ tesla), while the second one occurs at $b \approx 17\ \mu$eV ($B \approx 0.28$ tesla).

IV. SEQUENTIAL TRANSPORT THROUGH THE MOLECULE

We study electronic transport in our model system by connecting the molecule to two reservoirs of noninteracting electrons. The current through the molecule can be controlled by applying a voltage difference between the reservoirs, as well as by changing the total charge of the molecule through an applied backgate voltage. In order to evaluate single-electron transport, it is necessary to diagonalize the Hamiltonian for configurations with different total charge (i.e., different number of valence electrons in the ions). For simplicity, we only consider two charge states and we define $(N = 0, S = 2)$ as our initial state. In this state, the molecule has a $3d^8 - 2p^6 - 3d^8$ electronic configuration. Here, S denotes the total spin of the molecule. We then allow one electron to hop from the reservoirs into the molecule and restrict it to be localized either on the a_1 or c_1 orbitals, bringing the molecule to the $(N = 1, S = 3/2)$ state, which comprises both $3d^9 - 2p^6 - 3d^8$ and $3d^8 - 2p^6 - 3d^9$ electronic configurations. We assume that the coupling to the reservoirs is such that there is equal probability for an electron to land in either one of the two magnetic ions. Since one of the ions changes its oxidation state when an electron is added, its uniaxial anisotropy terms and the g-factors change as well. We take into account some of these changes in the Hamiltonian for the $S = 3/2$ configura-

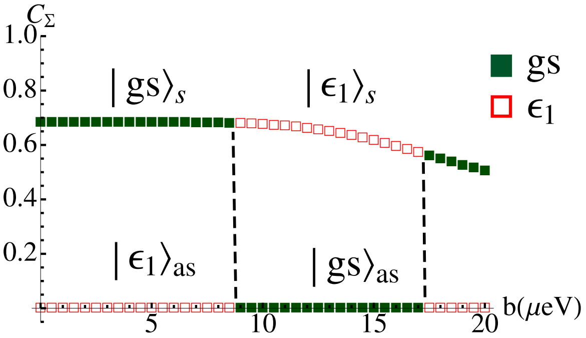

Figure 6: (Color online) Symmetry of the ground state (filled squares) and first excited state (empty squares) versus the magnetic field magnitude b. At $b = 0$ the ground and first excited states are $|\mathrm{gs}\rangle = 0.68(|{+2}\rangle + |{-2}\rangle) + 0.27\times$(contam.) and $|\epsilon_1\rangle = -0.69(|+2\rangle - |-2\rangle) + 0.22 \times$ (contam.), respectively, where (contam.) represents a contribution from spin states other than $|\pm 2\rangle$. Notice that as the transverse magnetic field grows, the amplitude C_Σ tends to decrease, allowing for an increasing admixture with $S_z = 0$ states. At the second diabolical point (right dashed line), the symmetry of the states changes again.

tion. Following Refs. 13 and 28, we assume a reduction in the uniaxial anisotropy and choose $d^{N=1} = d/2$. Notice that although the parameter $e^{N=1}$ is nonzero, it is not relevant to the ion receiving one electron since its total spin becomes $S_\alpha = 1/2$. For $S_\alpha = 1/2$, the local ground state of the ion is a Kramers' doublet, thus $e^{N=1}$ does not take part in the Hamiltonian for the $(N = 1, S = 3/2)$ configuration. In the literature,[29] there are indications that the anisotropic g factors may take a different value for the $(N = 1, S = 3/2)$ configuration. However, we do not expect the change to be significant and therefore, for the sake of simplicity, we assume the same g factors used for the $(N = 0, S = 2)$ configuration.

The general recipe for evaluating sequential, incoherent transport is to solve a set of coupled differential equations for the time evolution of the quantum state probabilities of the molecule. The standard rate equation for time evolution of the probability of an arbitrary state is given by[30]

$$\frac{dp_\alpha}{dt} = -p_\alpha \sum_\gamma \Gamma_{\alpha\to\gamma} + \sum_\gamma p_\gamma\, \Gamma_{\gamma\to\alpha}, \tag{9}$$

where $\Gamma_{\alpha\to\gamma}$ is the transition rate between different charge states α and γ and vice versa. The meaning of the right-hand side of the equation is the following. The first term comprises outgoing terms describing the transition from the initial state α to a state γ by means of taking away or adding an extra electron. The second term on the right-hand side of Eq. (9) represents processes where an initial state γ transitions to the final state α (again, by means of taking away or adding an extra electron). Equation (9) can be written in a matrix form

$$\frac{d\mathbf{P}}{dt} = \mathbf{\Gamma}\cdot\mathbf{P}, \tag{10}$$

where $\mathbf{P}$ is a vector containing the probabilities $\{p_\alpha\}$ and the matrix $\mathbf{\Gamma}$ contains elements $\{\Gamma_{\alpha\gamma}\}$ such that

$$\begin{aligned} \Gamma_{\alpha\gamma} &= \Gamma_{\gamma\to\alpha} \qquad \text{if} \qquad \alpha \neq \gamma \\ \Gamma_{\alpha\alpha} &= -\sum_{\gamma\neq\alpha} \Gamma_{\alpha\to\gamma}. \end{aligned} \tag{11}$$

In the stationary regime, we look for the steady-state probabilities p_α, this is, when $dp_\alpha/dt = 0$. In matrix form, this is achieved by determining the eigenvector $\mathbf{P}$ of the matrix $\mathbf{\Gamma}$ with a zero eigenvalue. The transition rates from a state α to a state γ when adding (or subtracting) electrons (e^-) to (from) the molecule are given by

$$\Gamma^\tau_{\alpha\to\gamma} = \begin{cases} \gamma^\tau_{\alpha,\gamma}\, f_\tau(\mu_{\alpha\gamma} - eV_\tau), & e^- \text{ in}, \\ \gamma^\tau_{\alpha,\gamma}\, \left[1 - f_\tau(\mu_{\alpha\gamma} - eV_\tau)\right], & e^- \text{ out}, \end{cases} \tag{12}$$

where the index $\tau = L, R$ refers to the left and right reservoirs, respectively. Here, $f_\tau(x) = 1/(1 + e^{\beta x})$ is the Fermi distribution of the left (L) or right (R) reservoirs. The electrochemical potential of the molecule, i.e., the energy required to go from a state α to state a γ, is defined as

$$\mu_{\alpha\gamma} = \epsilon_\alpha - \epsilon_\gamma - e\eta V_g, \tag{13}$$

where ϵ_α and ϵ_γ are the energy eigenvalues corresponding to the states α and γ, respectively, and V_g is the backgate voltage (we set the lever arm coefficient $\eta = 1$). We denote the splitting between eigenstates as $\Delta_{\alpha\gamma} = \epsilon_\alpha - \epsilon_\gamma$. The coefficients $\gamma^\tau_{\alpha,\gamma}$ are the tunneling rates between eigenstates of the molecule and are given in the Golden rule approximation by

$$\gamma^\tau_{\alpha,\gamma} = \begin{cases} 2\pi\rho \sum_\sigma |T^{\sigma,\tau}_{\alpha\gamma}|^2, & e^- \text{ in}, \\ 2\pi\rho \sum_\sigma |T^{\sigma,\tau}_{\gamma\alpha}|^2, & e^- \text{ out}, \end{cases} \tag{14}$$

where ρ is the reservoir's density of states and

$$T^{\sigma,\tau}_{\alpha\gamma} = \sum_j t_{j,\tau} \langle\alpha|c^\dagger_{j\sigma}|\gamma\rangle \tag{15}$$

denote the tunneling matrix elements. The operator $c^\dagger_{j\sigma}$ creates an electron with spin σ on the single-particle orbital j. To simplify the calculations we assume that $t_{j,\tau}$ is independent of the orbital, so we drop the j index. Since different charge configurations of the molecule involve states with different spin quantum numbers, selection rules for spin transitions become important in the transport calculations. The tunneling matrix elements satisfy the selection rules $|S_\alpha - S_\gamma| = 1/2$, $|S_{z\alpha} - S_{z\gamma}| = 1/2$ and $|N_\alpha - N_\gamma| = 1$, for any two eigenstates of the Hamiltonian. The current through the left lead is given by

$$I_L = |e| \sum_{\alpha\gamma} \Gamma^L_{\alpha\to\gamma} p_\alpha, \tag{16}$$

where α, γ are indexes for different charge states. The expression for the current is multiplied by 1 if the molecule is receiving an electron and by -1 if an electron is going out to the left reservoir.

V. BERRY-PHASE INTERFERENCE EFFECTS ON THE TRANSPORT

In order to see signatures of Berry-phase interference in the molecule's electronic transport, we consider only transitions between the two lowest energy levels of each spin-charge sector, as shown in Fig. 7. Since the energy levels for the $(N = 0, S = 1)$ and $(N = 1, S = 3/2)$ configurations are linear combinations of $|S_z = \pm 2\rangle$ and $|S_z = \pm 3/2\rangle$ states, respectively, the corresponding selection rules are trivially fulfilled and transitions between all states are possible at $b = 0$.

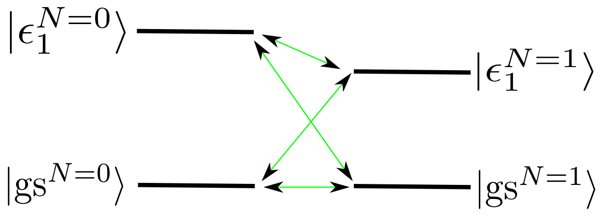
$|\epsilon_1^{N=0}\rangle$
$|\epsilon_1^{N=1}\rangle$
$|\mathrm{gs}^{N=0}\rangle$
$|\mathrm{gs}^{N=1}\rangle$

Figure 7: (Color online) The two lowest energy levels for the $N = 0$ and $N = 1$ charge sectors, with total spins $S = 2$ and $S = 3/2$, respectively. The arrows denote allowed transitions for $b = 0$.

It is worth noticing that although we choose only the two lowest energy levels, interesting physics beyond the reach of the GSA can be found if all combinations of S_z states corresponding to a particular total spin S of a molecule are considered. This is because anisotropy contributions tend to contaminate the lowest energy levels with a small admixture of $S_z = 0$ states, opening transitions in the transport that would otherwise have been forbidden by selection rules. An interesting study of these contributions to transport can be found in Ref. 16. Since we are primarily interested in how the modulation of the transverse anisotropy splitting affects transport, we only consider the two lowest energy S_z states. For other states, the energy cost to access different transitions would be too large compared to the splittings generated by the transverse anisotropy.

Because the splitting of the two lowest states due to transverse anisotropy for each charge sector is very small, of the order of μeV (see Fig. 8), a very small temperature is required to resolve features in the electronic transport that can be associated to Berry-phase interference. Thus, we set the temperature in the reservoirs to $T = 0.5$ mK. In order to bring the Berry-phase interference effects to higher temperature ranges, we attempted to increase the tunneling splitting rates by moving slightly away from the critical angle where the diabolical point develops. Unfortunately, we found that the splittings for the two spin-charge sectors grow at the same rate with the applied magnetic field, and their difference (which is the primary scale controlling the Berry phase interference effects), did not increase significantly. Thus, from an experimental perspective, it may be rather difficult to resolve all transport resonances in molecules with transition metal ion cores.

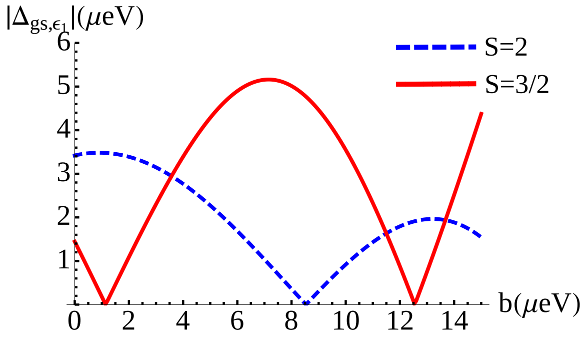

Figure 8: Splittings between the two lowest energy levels of the $S = 3/2$ (solid line) and $S = 2$ (dashed line) total spin sectors. We observe that $\Delta_{S=3/2} < \Delta_{S=2}$. The first diabolical point for $S = 3/2$ is at $b_{3/2} \approx 1.21$ μeV (equivalent to 0.02 T).

For the transport calculation, we tune the gate voltage to $V_g(b) = \epsilon_{\mathrm{gs}}^{N=1}(b) - \epsilon_{\mathrm{gs}}^{N=0}(b)$ so that the ground states energies for both spin-charge sectors are aligned. We set the density of states of the reservoirs and the tunneling coupling to arbitrary constant values. Transport is evaluated at $b = 0$ and $b = b_{3/2}$, the latter denoting the magnitude b_S of the field for which a diabolical point occurs for the spin-charge sector with total spin $S = 3/2$. The left-lead current I_L and the corresponding differential conductance (dI_L/dV) are shown in Figs. 9 and 10, respectively (the subscript L is omitted in the plots).

When the magnetic field is zero $(b = 0)$, transitions between excited states and between ground to excited states in different sectors can be appreciable in the last three steps of the current in Fig.9, which occur at $V_b \approx 33.5, 45.8, 79.9$ (in units of k_BT/e). The steps in Fig. 9 correspond to the linear conductance peaks in Fig. 10. As the magnetic field is tuned to the $S = 3/2$ diabolical point, the degeneracy of the $S_z = 3/2$ states is restored, suppressing the $|\epsilon_1^{N=0}\rangle \leftrightarrow |\epsilon_1^{N=1}\rangle$ and $|\mathrm{gs}^{N=0}\rangle \leftrightarrow |\epsilon_1^{N=1}\rangle$ transitions. This suppression is clearly visible in gray plots of dI/dV versus bias and gate voltages (Figs. 11 and 12). In Fig.11 the positive and negative slope lines corresponding to the $|\epsilon_1^{N=0}\rangle \leftrightarrow |\epsilon_1^{N=1}\rangle$ and $|\mathrm{gs}^{N=0}\rangle \leftrightarrow |\epsilon_1^{N=1}\rangle$ transitions, respectively, are eliminated, as shown in Fig. 12. The effect of the field therefore, is to allow current to go in or out of the molecule only if it is between ground states of the molecule or if $|\mathrm{gs}^{N=1}\rangle \leftrightarrow |\epsilon_1^{N=0}\rangle$ takes place. The latter corresponds to the surviving positive slope line in Fig. 12.

In Fig. 10, we also notice that a shift in the conductance peaks occurs for the transition between ground and first excited states of the $N = 1$ and $N = 0$ charge states. This is because the splitting of the $N = 0$ charge sector also varies with the application of the field (see Fig. 8). The field also causes a shift of the charge degeneracy point in Fig. 12. Since our choice of temperature is rather small, the increments of the gate voltage in the gray plots are very small. Thus, to improve visibility of

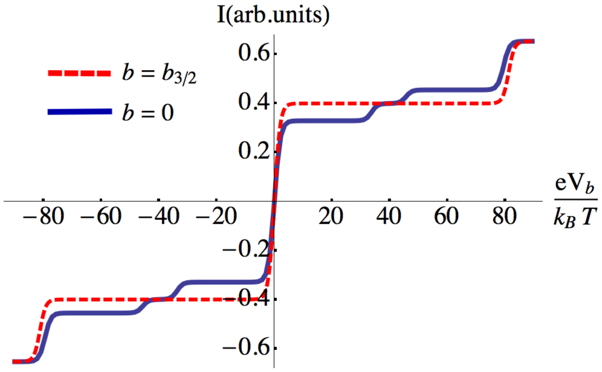

Figure 9: Current through left lead versus bias voltage at $b = 0$ (solid line) and $b = b_{3/2}$ (dashed line) for $T = 0.5$ mK (current shown in arbitrary units). The bias voltage is plotted in units of $k_B T/|e|$. We observe that the resonances at $V_b = \pm 33.5, \pm 45.8$ (in units of $k_B T/|e|$), which are present for $b = 0$, are eliminated due to the Berry-phase interference when $b = b_{3/2}$

the data, we shifted the gate voltage. The numerical values for the gate voltage axis correspond to the rescaling $e(V_\text{g} - V_s)/k_B T$ where $eV_\text{s} = 13.175$ eV.

VI. CONCLUSION

We have studied the incoherent electronic transport through an anisotropic magnetic molecule using a simple microscopic model that provides spectral properties similar to those of a multi-ion single-molecule magnet but also goes beyond the giant spin model. Our results show that at very low temperatures certain transitions are suppressed when an external in-plane magnetic field is tuned to a special direction and value. This suppression can be interpreted as the result of destructive interference of a topological phase – the Berry phase – as the total magnetization of the molecule transits between two opposite orientations.

The fact that we have to rely on very low temperature (in the submilikelvin range) to visualize features attributed to the Berry-phase interference indicates that they will be difficult to observe experimentally. However, for real single-molecule magnets with a multi-ion core, the energy scales controlling these features could easily increase by an order of magnitude. Thus, in practice, the situation should be more accessible than what our model calculations indicate. When searching for Berry-phase effects in transport, one should consider studying molecules

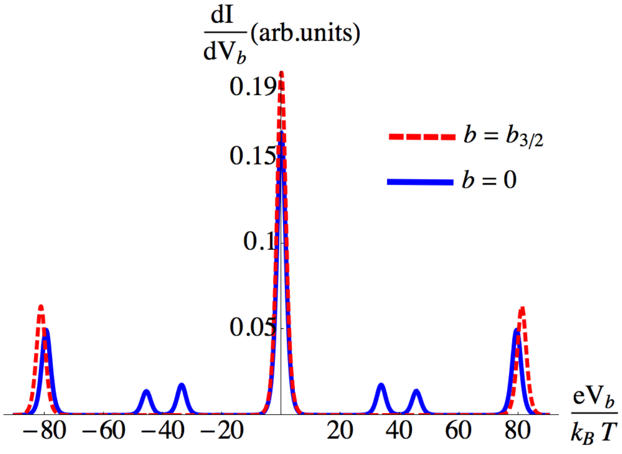

Figure 10: Plot of the differential conductance, dI/dV_b, as a function of bias voltage at $b = b_{3/2}$ (dashed line) and for $b = 0$ (solid line). The differential conductance is given in arbitrary units.

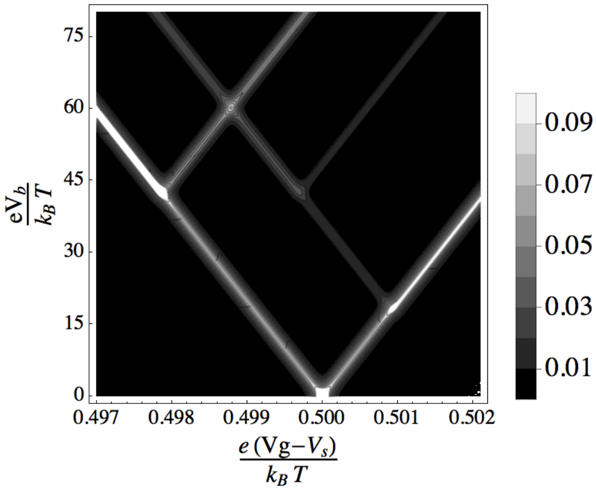

Figure 11: Gray plot of the differential conductance, dI/dV_b, as a function of bias and gate voltage at $b = 0$. The gate voltage is shifted by $V_s = 13.175$ V, as explained in the main text.

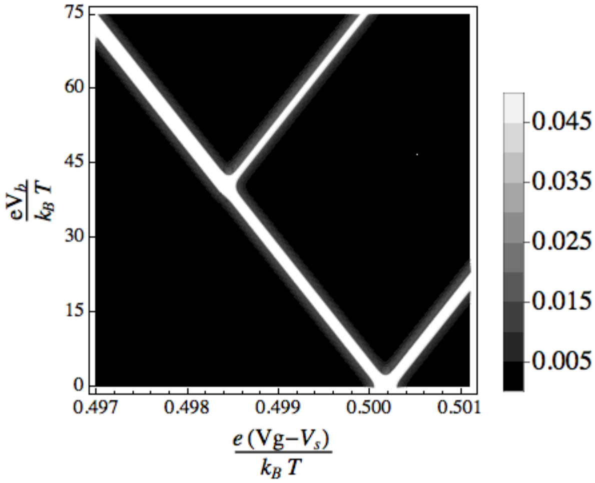

Figure 12: Gray plot of the differential conductance, dI/dV (in arbitrary units), as a function of bias and gate voltage at $b = b_{3/2}$. The gate voltage is shifted by $V_s = 13.175$ V, as explained in the main text.

with a large tunnel splitting (which most likely will require a relatively strong in-plane anisotropy as compared to the uniaxial anisotropy).

We plan to further explore our microscopic formulation to consider more complex molecules with multi-ion transition-metal cores. We are currently extending our approach to investigate Berry-phase effects in the electronic transport of mononuclear (single-ion magnets), which consist of just one rare-earth ion within a ligand cage. These systems have been synthesized with success in recent years (see for instance Refs. 31–34).

Acknowledgments

This work was supported by NSF ECCS under Grant No. 1001755. The authors would like to thank Enrique del Barco, George Martins, and Edson Vernek for valuable comments.

---

[*] Electronic address: jromerobohorquez@knights.ucf.edu

[†] Electronic address: mucciolo@physics.ucf.edu

[1] G. Christou, D. Gatteschi, D. N. Hendrickson, and R. Sessoli, MRS Bulletin **25**, 66 (2000).
[2] D. Gatteschi, R. Sessoli, and J. Villain, *Molecular Nanomagnets* (Oxford University Press, New York, 2007).
[3] J. Friedman and M. P. Sarachik, Annu. Rev. Condens. Matter. Phys. **1**, 109 (2010).
[4] J. R. Friedman, M. P. Sarachik, J. Tejada, and R. Ziolo, Phys. Rev. Lett. **76**, 3830 (1996).
[5] L. Thomas, F. Lionti, R. Ballou, D. Gatteschi, R. Sessoli, and B. Barbara, Nature (London) **383**, 145 (1996).
[6] A. Ardavan *et al.*, Phys. Rev. Lett **98**, 057201 (2007).
[7] W. Wernsdorfer and R. Sessoli, Science **284**, 133 (1999).
[8] H. M. Quddusi *et al.*, Phys. Rev. Lett. **106**, 227201 (2011).
[9] S. Hill *et al.*, Dalton Trans. **39**, 4693 (2010).
[10] J. B. Goodenough, Phys. Rev. **100**, 564 (1955).
[11] J. Kanamori, J. Phys. Chem. Solids **10**, 87 (1959).
[12] P. W. Anderson, Phys. Rev. **79**, 350 (1950).
[13] C. Romeike, M. R. Wegewijs, and H. Schoeller, Phys. Rev. Lett. **96**, 196805 (2006).
[14] G. Gonzalez and M. N. Leuenberger, Phys. Rev. Lett. **98**, 256804 (2006).
[15] M. N. Leuenberger and E. R. Mucciolo, Phys. Rev. Lett. **97**, 126601 (2006).
[16] C. Romeike, M. R. Wegewijs, W. Hofstetter, and H. Schoeller Phys. Rev. Lett. **96**, 196601 (2006)
[17] G. Gonzalez, M. N. Leuenberger, and E. R. Mucciolo, Phys. Rev. B **78**, 054445 (2008).
[18] K. Park, E.-C. Yang, and D. N. Hendrickson, J. Appl. Phys. **97**, 10M522 (2005).
[19] S. Barraza-Lopez, K. Park, V. Garcia-Suarez, and J. Ferrer, Phys. Rev. Lett. **102**, 246801 (2009).
[20] K. Park, S. Barraza-Lopez, V. M. Garcia-Suarez, and J. Ferrer, Phys. Rev. B **81**, 125447 (2010).
[21] J. F. Nossa, M. F. Islam, C. M. Canali, and M. R. Pederson, Phys. Rev. B **85**, 085427 (2012).
[22] M. V. Berry, and M. Wilkinson, Proc. R. Soc. London A, **392**, 15 (1984).
[23] M. Imada, A. Fujimori, and Y. Tokura, Rev. Mod. Phys. **70**, 1039 (1998).
[24] B. H. Kim and B. I. Min, New J. Phys. **13**, 073034 (2011).
[25] Z.-H. Zhang *et al.*, Mod. Phys. Lett. B **23**, 1415 (2009).
[26] F. Wang *et al.*, J. Magn. Magn. Mat. **329**, 88 (2013).
[27] A. Garg, Europhys. Lett. **22**, 205 (1993).
[28] R. Basler *et al.*, Inorg. Chem. **44**, 649 (2005).
[29] W. L. Feng *et al.*, J. Magn. Magn. Mater. **323**, 528 (2011)
[30] C. W. J. Beenakker, Phys. Rev. B **44**, 1646 (1991).
[31] M. A. Aldamen *et al.*, J. Am. Chem. Soc. **130**, 8874 (2008).
[32] M. A. Aldamen *et al.*, Inorg. Chem. **48**, 3467(2009).
[33] J. Titel *et al.*, J. Am. Chem. Soc. **133**, 15814 (2011).
[34] M. Martinez-Perez *et al.*, Phys. Rev. Lett. **108**, 247213 (2012).